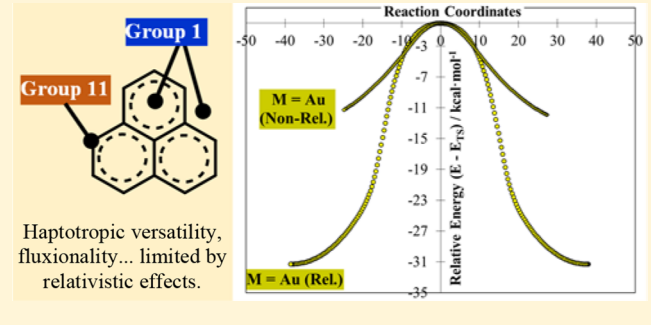
Hop-Skip-Jump: Monovalent Metals on the Surface of the Phenalenyl Radical

Supreeth Prasad, Noah Walker, Michael Henry, and Kelling J. Donald*

Department of Chemistry, Gottwald Center for the Sciences, University of Richmond, Richmond, Virginia 23173, United States

Supporting Information

ABSTRACT: The phenalenyl radical (P) and its relatively stable cation and anion are of interest for applications in areas spanning magnetic materials and ligand development for reaction catalysis. We report on a broad investigation of the bonding, thermochemistry, and kinetics of PM complexes where M is a group 1 or 11 metal atom. The PM species that are considered in this work afford a simplified picture of the behavior of metal adatoms on hydrogen terminated graphene fragments, and, more crucially, we expand a still nascent understanding of the organometallic chemistry of P. The exceptional fluxionality of group 1 metals on the phenalenyl



surface is predicted, the associated energy barriers are quantified, and the major role of relativistic effects in restricting the fluxionality of Au on the surface is demonstrated. Although relativistic effects swell the barriers to isomerization, we find that orbital size and energies, even in the absence of relativistic effects, dictate different path preferences for the motion of Au on the surface of the radical compared to Cu and Ag.

INTRODUCTION

The phenalenyl radical, P, continues to attract attention at the intersections of chemistry and molecular physics. That is largely because of the relatively long lifetime of the radical and the stability of its cation and anion 1-4—and much of that versatility is rooted in the nature of its nonbonding singly occupied molecular orbital (SOMO) depicted in Figure 1a.

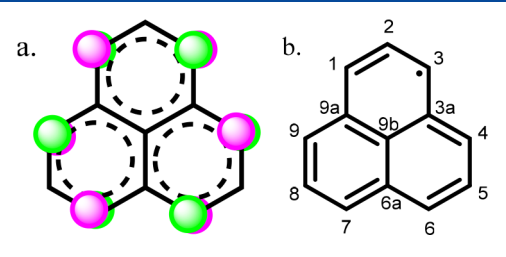


Figure 1. Models of (a) the SOMO and (b) a resonance form for the radical. Other symmetrically identical resonance forms can be drawn. The resonance form with the radical electron at C(9b) is disfavored; the SOMO has a node at C(9b).

Apart from the resonance form shown in Figure 1b, a number of symmetrically identical localized representations can be drawn for the radical in which the unpaired electron is positioned at another one of the secondary α -carbon centers involved in the SOMO. A distinct alternative canonical form locates the radical electron on the central carbon atom (C(9b) in Figure 1b), but that representation is inconsistent with the distribution of the electron density in the SOMO (Figure 1a), which has a node at C(9b).

The phenalenyl radical is the simplest polycyclic hydrocarbon (n = 2) in the n-triangulene radical series, $C_{n^2+4n+1} H_{3n+3}$ (for n = 2, 3, 4, ...), ^{5,6} and its properties as a relatively small and persistent polycyclic radical have already earned it some utility in a number of active areas of research: The cation has been shown, for instance, to be an influential (noninnocent) ligand fragment in the catalysis of a hydroamination reaction, 4,7 and the radical has been examined in the ongoing development of reliable organic conductors and spin memory devices. 4,8,5

Yet progress in the organometallic chemistry of the radical has been rather slow. A practical limitation for the unsubstituted radical as a reagent is that it tends to dimerize or react otherwise rather easily, $^{1-3,10-12}$ but it has been known for some time that the stability of the radical can be enhanced by substitutions for more bulky substituents on the ring. Experimentally characterized examples of the substituted radical include perchlorophenalenyl, ¹³ and (2,5,8-trisubstituted) *tert*-butyl-, ¹⁴ methyl-, ¹⁵ phenyl-, ¹⁵ and pentafluorophenyl-16 phenalenyl.

In a previous contribution, 17 our group examined full sandwich complexes of the phenalenyl radical for a series of main group and d-block metals. We are interested broadly in developing an improved fundamental understanding of the physical and organometallic chemistry of metal complexes of polycyclic rings, and we consider in this work the structure, bonding, energetics, and fluxionality of monovalent (groups 1 and 11) phenalenyl-metal systems. To the extent that the

Received: August 19, 2019 Published: December 24, 2019

phenalenyl radical approximates a hydrogen terminated fragment of a graphene sheet, this investigation provides some insights into the behavior of adatoms on graphitic surfaces as well. The monovalent metal atoms provide a unique opportunity for an assessment of the structural chemistry of the phenalenyl complexes since the PM(I) molecules are expected, without ambiguity, to be closed shell systems. For the group 11 systems, we find unique modes of motion across the surface of P. Compared to those late d-block systems, however, the group 1 species are extremely fluxional and tend to prefer positions on the phenalenyl ring that maximize hapticities. For Au, relativistic effects are found to account for an inordinate fraction of the barriers to motion about the surface of P.

The broad questions of the behavior of polycyclic radicals as ligands and the behavior of metal atoms on two-dimensional materials intersect in this work. We focus in this investigation on the groups 1 and 11 metals and the electronically beguiling phenalenyl ring as simple models for the behavior of metal atoms on the surfaces of polycyclic graphitic fragments.

■ RESULTS AND DISCUSSION

The outcomes of an investigation of the structural preferences, bonding, and energetics of monovalent groups 1 and 11 metal atoms (M = Li, Na, K, Rb, Cs, Cu, Ag, and Au) on the surface of the phenalenyl ring are summarized in Figure 2. Our results

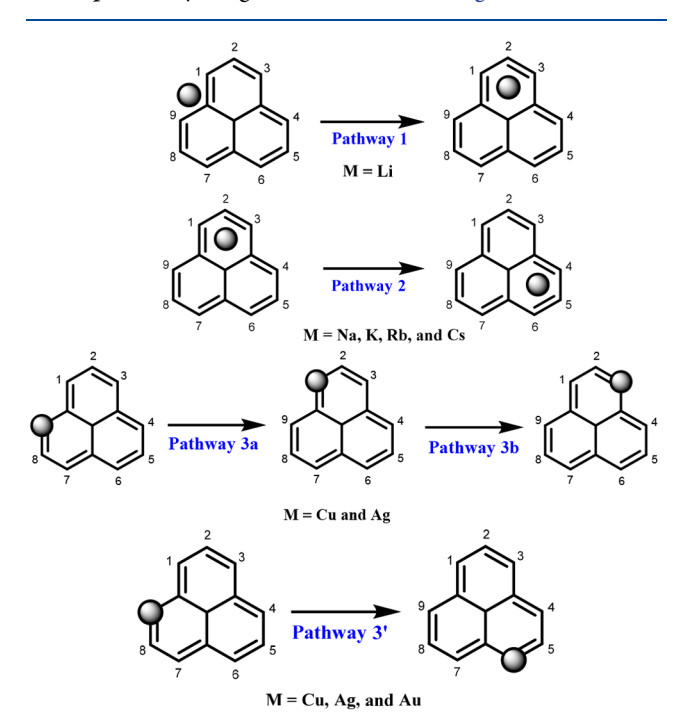


Figure 2. Representations of structural preferences of groups 1 and 11 phenalenyl metal complexes. The arrows indicate that we have traced pathways linking the minima shown. Pathways 3 (= 3a + 3b) and 3' are both accessible to Cu and Ag. The pathways are discussed in the text.

reveal a diverse set of minimum energy geometries for the metal atoms on the singlet potential energy surface of *PM*, with the hapticities and the positions of the metal centers depending on the identity of M. Since the specific values of the geometrical parameters vary widely from one metal atom to the next, only the general positions of the M atoms are

indicated (depicted in each case by a gray sphere) in Figure 2. Ball and stick models of the optimized structures, Cartesian coordinates, and key structural parameters for each species are included in Table S1–S6 and visualization (.xyz) files in the Supporting Information (SI). We include arrows between the minimum energy structures in Figure 2 in preparation for a later discussion of barriers to isomerization (i.e., haptotropic rearrangements) for M around or across the surface of the phenalenyl ring. But first, a few words on the general structural preferences in the complexes.

Group 1 PM Systems: Structure and Bonding. The phenalenyllithium (*PLi*) species is unique among the group 1 systems, adopting a somewhat different set of minimum energy geometries compared to heavier group 1 cases.

Two local minima were identified for PLi: (i) an η^3 species with the Li atom above the recess or bay-like area at the intersection of two six-membered rings, and (ii) an η^6 alternative with Li above one of the six-membered rings (see Figure 2; Pathway 1). We have had to rely completely on the position of M and its proximity to adjacent C centers for our assessment of the hapticities (see Table S6). For covalently bound systems, the bond order between two atoms or fragments is arguably a better measure of the extent of the bonding, but the PLi system is extremely polar: the strongly positive point charges obtained for Li in PLi from a natural bond orbital analysis (Table 1) are +0.88e (η^3) and +0.88e

Table 1. NBO Point Charges, Total Wiberg Bond Indices (WBIs), and (Homolytic and Heterolytic) Binding Free Energies for Group 1 η^6 (Plus η^3 Case for Li) and Group 11 η^1 Minimum Energy PM Species

			binding free energies: ΔG (298.15)/kcal·mol ⁻¹		
M	charge	WBI	$\frac{G(PM) - G(P) - G(M)}{G(M)}$	$G(PM) - G(P^{-}) - G(M^{+})$	
Li (η^3)	+0.88	0.23	-24.8	-123.7	
Li (η^6)	+0.88	0.24	-32.4	-131.2	
Na	+0.96	0.09	-15.4	-107.6	
K	+0.93	0.16	-24.0	-96.2	
Rb	+0.93	0.15	-25.3	-93.0	
Cs	+0.92	0.18	-29.0	-89.6	
Cu	+0.42	0.94	-7.1	-158.3	
Ag	+0.33	0.99	+1.9	-148.9	
Au	+0.08	1.14	-10.2	-196.1	

 (η^6) . And the corresponding bond indices (for contacts between Li and atomic centers in *P*) are accordingly quite low: 0.23 (η^3) and 0.24 (η^6) (Table 1).

For complexes of the heavier group 1 atoms, only η^6 structures (Figure 2; Pathway 2) were found to be local minima on the *PM* surface, even if the M atom tends to drift in toward the central C(9b) atom as M gets larger (Table S6). The η^6 hapticity was obtained even when we started structural optimizations specifically from η^3 -type arrangements with the M centers over the recess area. And those η^6 species—even more so than for *PLi* (Table 1)—exhibit remarkably high degrees of polarity in their bonds to the phenalenyl rings (tending toward the P^-M^+ limit): the NBO charges at M, for instance, are between +0.92e to +0.97e (Table 1) for the larger group 1 metals and the bond orders are all <0.20 (see Table S6 for relevant individual M—C bond orders and distances).

The binding free energy data in Table 1, with values referenced to both the homolytic (neutral) and a heterolytic

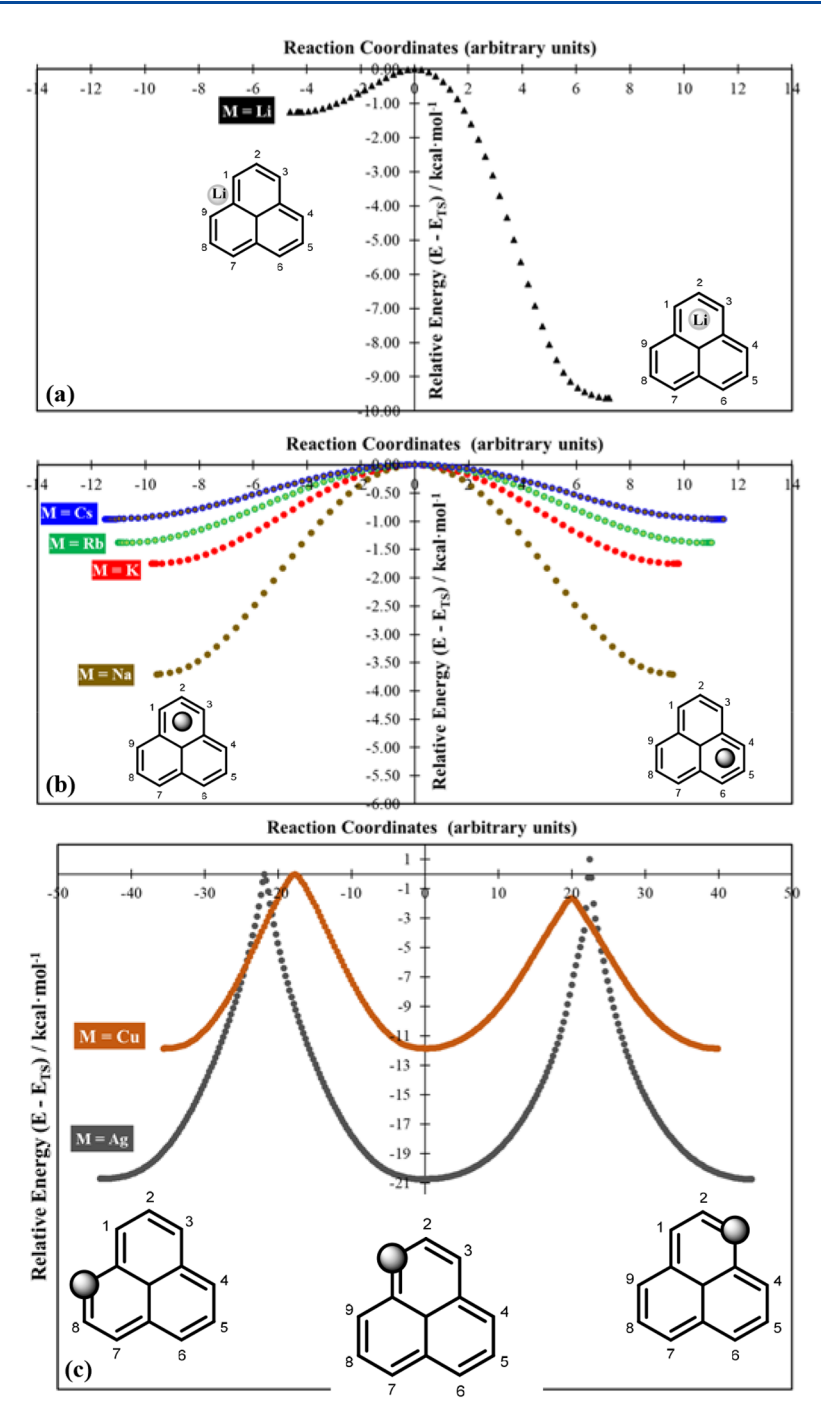


Figure 3. IRC paths for PM systems that follow (a) pathway 1 (M = Li), (b) pathway 2 (other group 1 metals), and (c) pathway 3 (Cu and Ag). All of the pathways terminate at symmetrically identical positions, except for Li, which changes hapticities ($\eta^3 \to \eta^6 \to \eta^3$ and so on) as it moves around the ring.

dissociation of PM, show that, by either measure, the η^6 Li and η^1 Au complexes have the highest binding energy of their respective series. Remarkably, in the homolytic case, the smallest value by far is obtained for M=Na, with ΔG increasing thereafter as we go down the group to Cs, where the binding energy is just over 3 kcal·mol^{-1} below that for PLi. We do not take up the question in this work, but an assessment of the dissociation of these complexes in solution may be in order, and the data provided here offer a starting point for that discussion.

Group 11 *PM* Systems: Structure and Bonding. The Cu, Ag, and Au atoms behave quite differently from the group 1 metals on the phenalenyl surface. Unrestrained energy minimizations of the *P*Cu, *P*Ag, and *P*Au systems lead inexorably to point saturations at a single secondary α -carbon on the edge of *P* as depicted in pathways 3 (= 3a + 3b), and 3' in Figure 2 (see Tables S3–S4 in the SI). Those are precisely the sites involved in the SOMO in Figure 1, so the radical is quenched through the direct formation of an M–C covalent bond, a situation that we have not observed for any of the group 1 metals where—notwithstanding some covalent

Organometallics Article Article

contributions to bonding—the P^-M^+ contribution dominates. ^{18,19} To be clear, those η^1 edge-bonding group 11 minimum energy structures were obtained even when the geometry optimizations were initiated with M in an η^6 position above one of the six-membered rings of P.

Relative to the gas phase $P^- + M^+$ reference fragments, the group 11 systems gain noticeably more from complex formation (i.e. ΔG is more negative in Table 1) than the group 1 cases, with PAu having the largest binding free energy $(-196.1 \text{ kcal·mol}^{-1})$. The gains for the group 11 systems are noticeably smaller than they are for the group 1 cases, however, when neutral reference fragments are considered: ΔG is actually slightly positive for M = Ag, and although $\Delta G(PAu) = -10.2 \text{ kcal·mol}^{-1}$ with the neutral references, it is still less negative compared to $-33.0 \text{ kcal·mol}^{-1} \leq \Delta G(PM) \leq -15.0 \text{ kcal·mol}^{-1}$ for the group 1 complexes. Here again, however, the relevant binding energy data set for consideration as a starting point for analysis will depend on the experimental context.

The covalent character of the η^1 bonds in the group 11 (*PM*) is confirmed by the point charge and bond order data in Table 1. For those systems, the point charges are quite low, all < +0.45e (only +0.08e for Au), and the Wiberg bond indices are high (Table 1). For M = Au, the bond index for the direct Au–C bond is 0.73 (Table S6), but smaller contributions from weak overlaps with neighboring sites contribute to an overall *PA*u bond index of 1.14 (Table 1).

A distinction is made in Figure 2 between pathways 3 and 3′ because of differences in how Au moves between minima on the phenalenyl surface compared to Cu and Ag—and we say more on that shortly—but the definite preferences for η^1 coordination at an α -carbon on the edge of P is common to all three of the group 11 PM systems.

Haptotropic Rearrangements in Groups 1 and 11 Metal-Phenalenyl Complexes (*PM(I)*). The barriers to the motion of group 1 atoms, Cu, and Ag, between minimum energy structures on their respective *PM* potential energy surfaces, which each follow pathway 1, 2, or 3, are shown in Figure 3. *P*Au is considered separately due to certain unique features of pathway 3' and exceptional characteristics of the phenalenylgold complex.

For each of the PM systems considered in this work, IRC paths have been obtained for the shortest sequence of hops, skips, or jumps—well-defined isomerizations or haptotropic rearrangements—along the potential energy surface that, with repetition, moves the M atom around or across the ring in an orderly way and back to any arbitrary starting point in the path. Structural representations and coordinates for the optimized end points and transition structures for each pathway are included in the Supporting Information (see Tables S1–S6 and the visualization files).

Group 1 Rearrangements: Pathways and Barriers. For M = Li, the simplest continuous motion from one minimum energy geometry to the next is a translocation between an η^3 coordination site above the recess region and an adjacent (and more stable) η^6 coordination site above the ring (Figure 3a; pathway 1 in Figure 2).

Attempts to directly link the η^6 minima for M = Li were unsuccessful. By symmetry, therefore, the lowest energy path for the motion of lithium around the ring involves apparently a sequence of shifts from recess region to ring to recess region and so on (i.e., $\eta^3 \to \eta^6 \to \eta^3$...) around P, and we show in Figure 3a the energy barriers associated with the minimal $\eta^3 \to \eta^6$ repeatable motion needed for Li to circumnavigate the ring.

The activation free energy $(\Delta G(Li)_{\ddagger}^{\eta^3-TS})$ separating the η^3 minimum from the TS for Li $(1.16 \text{ kcal·mol}^{-1})$ is \sim 7.5 times smaller than the barrier going from the η^6 minimum to the TS $(\Delta G(Li)_{\ddagger}^{\eta^6-TS}=8.76 \text{ kcal·mol}^{-1};$ see the ΔG^{\ddagger} values in Table 2). So the η^6 species is favored rather strongly by *P*Li relative to the η^3 form, though the actual barriers are not particularly high.

Table 2. Computed B3PW91 Energies (with Zero-Point Corrections ($\Delta E_{\rm ZPE}$)), and Free Energies (ΔG) at 298.15 K in kcal·mol⁻¹ for PM Minima Relative to Each Other, $\Delta E_{\rm ZPE}$ = $E_{\rm ZPE}({\rm Min.~1}) - E_{\rm ZPE}({\rm Min.~2})$, and Barriers Separating Each PM Minimum from the TS for the Relevant Pathway: $\Delta E_{\rm ZPE}^{\ddagger}(1) = E_{\rm ZPE}({\rm TS}) - E_{\rm ZPE}({\rm Min.~1})$, and Similarly for $\Delta E_{\rm ZPE}^{\ddagger}(2)$ and the Corresponding ΔG Values

	pathway	$\Delta E_{ m ZPE}$	$\Delta E^{\ddagger}_{ m ZPE}(1)$	$\Delta E^{\ddagger}_{ m ZPE}(2)$
Li	1	7.91	$0.98 (\eta^3)$	8.89 (η^6)
Na	2	0.00	3.38	3.38
K	2	0.00	1.58	1.58
Rb	2	0.00	1.20	1.20
Cs	2	0.00	0.84	0.84
Cu^b	3a; 3b	0.00; 0.00	10.51; 9.09	10.51; 9.09
Ag^b	3a; 3b	0.00; 0.00	19.03; 19.87	19.03; 19.87
Au	_	_	_	_
Cu	3′	0.00	17.24	17.24
Ag	3′	0.00	18.26	18.26
Au	3′	0.00	30.65	30.65
Ag (Nonrel) ^c	3′	0.00	12.36	12.36
Au (Nonrel) ^c	3′	0.00	12.46	12.46
	pathway	ΔG	$\Delta G^{\ddagger}(1)$	$\Delta G^{\ddagger}(2)$
Li	1	7.59	1.16	8.76
Na	2	0.00	3.51	3.51
Na K	2 2	0.00 0.00	3.51 2.05	3.51 2.05
K	2	0.00	2.05	2.05
K Rb	2 2	0.00 0.00	2.05 1.94	2.05 1.94
K Rb Cs	2 2 2	0.00 0.00 0.00	2.05 1.94 1.63	2.05 1.94 1.63
K Rb Cs Cu ^b	2 2 2 3a; 3b	0.00 0.00 0.00 0.00; <i>0.00</i>	2.05 1.94 1.63 11.26; 9.32	2.05 1.94 1.63 11.26; 9.32
K Rb Cs Cu ^b Ag ^b	2 2 2 3a; 3b	0.00 0.00 0.00 0.00; <i>0.00</i>	2.05 1.94 1.63 11.26; 9.32	2.05 1.94 1.63 11.26; 9.32
K Rb Cs Cu ^b Ag ^b Au	2 2 2 3a; 3b 3a; 3b	0.00 0.00 0.00 0.00; <i>0.00</i> 0.00; <i>0.00</i>	2.05 1.94 1.63 11.26; 9.32 19.62; 20.25	2.05 1.94 1.63 11.26; 9.32 19.62; 20.25
K Rb Cs Cu ^b Ag ^b Au Cu	2 2 2 3a; 3b 3a; 3b — 3'	0.00 0.00 0.00 0.00; <i>0.00</i> 0.00; <i>0.00</i> -	2.05 1.94 1.63 11.26; 9.32 19.62; 20.25 —	2.05 1.94 1.63 11.26; 9.32 19.62; 20.25 —
K Rb Cs Cu ^b Ag ^b Au Cu Ag	2 2 2 3a; 3b 3a; 3b - 3' 3'	0.00 0.00 0.00; 0.00 0.00; 0.00 - 0.00 0.00	2.05 1.94 1.63 11.26; 9.32 19.62; 20.25 — 17.59 18.37	2.05 1.94 1.63 11.26; 9.32 19.62; 20.25 — 17.59 18.37

^aMin.: confirmed minimum energy structures. ^bPathway 3b data in italics. ^cComputed using nonrelativistic basis sets and ECPs.

For the heavier group 1 metals, the shallow η^3 minimum vanishes completely. The η^6 structure with M above a sixmembered ring in P emerges as the undisputed global minimum for all of the group 1 atoms below Li in the periodic table. This observation is well in line with the established bonding preference of K, for instance, in potassium graphites²⁰ and the well-known bias of group 1 metals toward high hapticities in, for example, organo-metal¹⁸ and inorganic clusters.²¹ But those heavier PM systems are expected to be much more fluxional than the Li case, since their activation barriers are small $((\Delta G(Li)_{\frac{1}{4}}^{\rho^6-TS} \le 3.6 \text{ kcal·mol}^{-1})$ relative to $(\Delta G(Li)_{\frac{1}{4}}^{\rho^6-TS}$ for Li $(8.76 \text{ kcal·mol}^{-1})$, shrinking continuously as M gets heavier (see Figure 3 and Table 2). At even moderate temperatures, therefore, the mobility of the heaviest

group 1 metal atoms on the surface of P is expected to be substantial relative to their Li analogue.

The $\eta^3 \leftrightarrow \eta^6$ haptotropic rearrangement predicted for *PLi* in the gas phase, the implications of that rearrangement for the electronic structure, the possible persistence of both isomers in solution, and the predicted fluxionality of heavier group 1 *PMs* invite experimental investigation. The syntheses of these *PM* systems present the initial challenge, but the existence of CpM compounds^{22–24} offers some hope perhaps for the preparation of these more elaborate analogues.

Group 11 Rearrangements: Pathways and Barriers. The resistance of group 11 PM systems to fluxional behavior relative to the group 1 species is demonstrated in Figure 3. Graphs (a), (b), and (c) in Figure 3 have been plotted on different scales, in order to get good separation of the curves in (b) especially, but it is clear that the barriers to the translation of M across P are higher for Cu, and even more so for Ag, than they are for the group 1 metal atoms (see Figures S8–S10 for the corresponding values obtained at an alternative (ω B97XD) level of theory).

The higher barriers that we have observed for the group 11 metals are consequences, in part, of the nature of the bonding of those metals to P (a single, directed M–C covalent bond) compared to the high hapticity structures formed by the monovalent main group metals: The group 1 metals—having empty and accessible np orbitals available (and even (n-1)d orbitals starting at K) that can accept electron density from the ring—tend to form multicenter bonds any chance they get. Experimentally observed cyclopentadienyl-metal (CpM) species, for example, all feature η^5 coordination of M to the five membered ring. $^{22-24}$

Our results for the group 11 systems are consistent with previous observations for divalent sandwich complexes of the late first row d-block elements including P-Cu-P. 17 The latter system was found computationally to be an η^2, η^2 slipped sandwich structure in which the Cu(II) metal atom bonds to the edges of the two P rings. For group 11 metal atoms, their higher electronegativities (relative to the group 1 metal atoms at least), repulsion of electron densities of the π -electrons in the ring and the filled M d-orbitals, 25 and the lack of empty low-energy valence orbitals limits their options for achieving high hapticities with planar ring systems. That is not to say that high hapticities are impossible for group 11 metals, 26 but they are rare. An η^6 [Cu(I)C₆H₆]⁺ complex was claimed only about a year ago as an unprecedented case for Cu, for example, and was explained as a "taming" of the Cu complex by strategic ligand selection.²⁷ Without the aid of ligands on the group 11 metal centers, however, the strong preference for direct M-C single bond formation goes unchallenged. Interestingly, phenalene (PH, with saturation at a single α -carbon) is also believed to exhibit the same kind of "six-fold tautomerization"28 that arises with pathway 3 (Figure 2) as summed up in Figure 4a. In this respect, H aligns with group 11 over group 1.

Pathway 3' (Figure 2), a confirmed route by which the Au atom is able to move between minima across the PAu potential energy surface, is very different from Pathway 3. The basic trajectories associated with both pathways—starting arbitrarily in each cases at atom C(9) and moving around or across the ring—are summarized in Figure 4.

Unlike pathway 3, which involves shifts from one α -carbon to another, Pathway 3' involves a veritable jump from one carbon center (e.g., C(9) in Figure 4b) completely over one six-membered ring across the surface of P to an α -carbon on

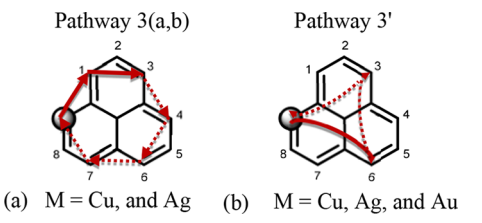


Figure 4. Summary of the trajectories involved in pathways (a) 3 and (b) 3'. The unbroken lines correspond to the paths traced out explicitly in Figures 3c and 5. The broken line shows how repeating those motions may move M eventually around to ring.

another six-membered ring (C(6)) in the structure (Figure 4b). That mode of isomerization (Pathway 3') is observed for M = Cu and Ag as well (Figure 5), but in those cases, the alternative edge-traversing pathway—Pathway 3—for translocation around the ring is also allowed (see Figure 3c). Indeed, the barriers for Pathway 3 are lower for M = Cu and comparable if slightly higher for M = Ag relative to the barriers for Pathway 3' (Figures 3b and 5; see Table 2).

For M = Au, for which pathway 3 is evidently inaccessible, the barrier for pathway 3' is higher by at least $10.0 \text{ kcal} \cdot \text{mol}^{-1}$ than the barriers obtained for Cu or Ag for either of the two pathways (Figures 3b and 5). By far, therefore, considering the group 1 metal phenalenyls as well, Au presents the most substantial barrier to ring-hopping or haptotropic rearrangements and is expected to be the least fluxional of the group 1 and 11 PM compounds.

Gold Anomaly. Futile searches for isomerization mechanisms for PAu that follow pathway 3 have convinced us that such a pathway is hindered if not forbidden for Au. An effort to locate direct paths around the edge of P that are analogous to stages 3a and 3b, for example (Figure 2), either returned us to the transition structure for pathway 3' or to a trans-plane or face-change isomerization. In the latter case, the Au atom actually goes below the plane of P through a planar transition state (Figure 6), to form an isostructural η^1 species with the new M—C single bond on the opposite face of the ring (see also an animation of the IRC path included in the SI).

Indeed, an attempt to model stages 3a and 3b by employing potential energy surface scans instead of IRC calculations led, in both cases, to evidence of a significant resistance to any direct shift from, for example, C(9) to C(1) or C(7) for PAu (see Figures 4a). The outcomes of the scans are shown in Figure S5, with the Au–C bond exchange occurring only after the progressive reduction of the Au–C separation obliged it.

How though to account for these exceptional features of the gold system? The relatively high barrier for the translocation of Au on the surface of P is consistent with the relativistic s-orbital stabilization and the relatively high bond dissociation energies that are expected for Au(1) covalent compounds, ^{29,30} especially when Au is bonded to a more electropositive atoms. ⁴¹ And Figure 7 illustrates the exceptional contribution that relativistic effects makes to that barrier.

To assess the influence of relativistic effects, we optimized the relativistic transition state at a nonrelativistic level of theory, deploying the Stuttgart—Cologne MHF nonrelativistic basis set and ECP for M = Au, instead of the relativistic MDF alternative. That transition state structure was qualitatively similar to the relativistic version for pathway 3', and produced an IRC path that linked the same starting and final geometries (a shift from C(9) to C(6); Figure 7) as those obtained with

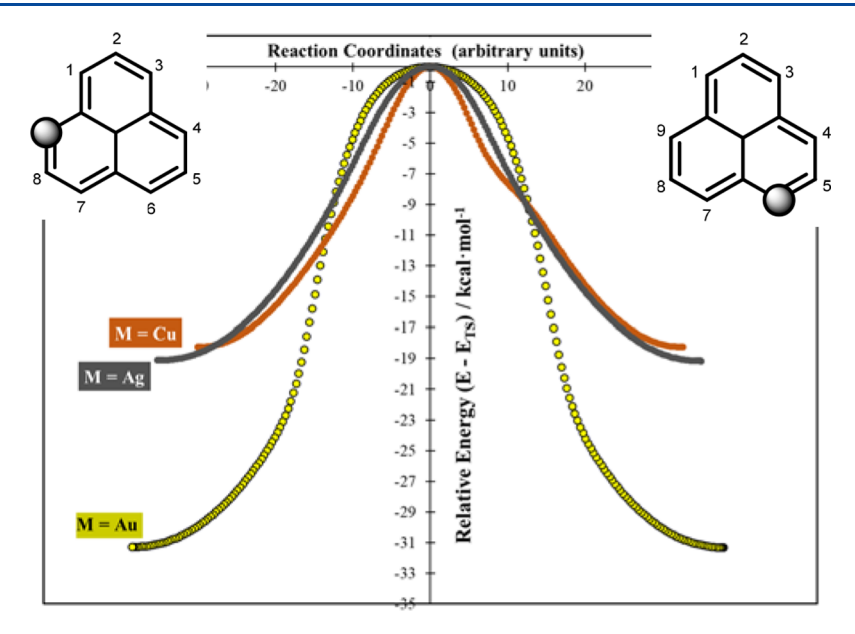


Figure 5. IRC paths for PCu, PAg, and PAu following Pathway 3'.

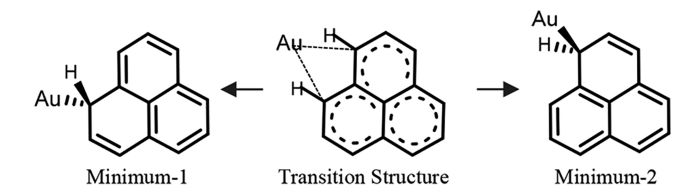


Figure 6. A "face-change" transplanar isomerization mechanism observed for M = Au. In the transition structure, the Au and adjacent H atoms are roughly coplanar with the ring.

the relativistic calculations for pathway 3' (see Figure 7 and Tables S4 and S5). What was different between the relativistic and nonrelativistic calculations, however, was the barrier to the shift of the Au atom (Figure 4b). The nonrelativistic barrier is well under half of the value for relativistic equivalent (see Figure 7, and Table 2). For M = Ag, the decrease in the

activation barrier in the absence of relativistic contributions is much smaller ($\Delta\Delta G^{\ddagger}=5.5~\text{kcal}\cdot\text{mol}^{-1}$; See Table 2 and Figure S1 and S10). So relativistic effects account for an exceptionally large barrier in pathway 3' for Au (compared to the Ag case), but those effects still do not account, we find, for the apparent unavailability of pathway 3 to Au.

A search for a gold transition state for pathway 3 using even the nonrelativistic option as we just mentioned led us back to the TS for pathway 3', but we looked elsewhere as well for explanations for the strong preference in PAu for route 3' and the avoidance of route 3.

An assessment of the lowest vibrational frequencies for PCu, PAg, and PAu turns out to be quite instructive. Consider Figure 4. The two lowest frequencies (molecular vibrations) for all three group 11 PM complexes correspond to rocking motions of the η^1 C(9)-M bond that move the M atom (i) toward C(6) on the other side of P in one case (Figures 4b,

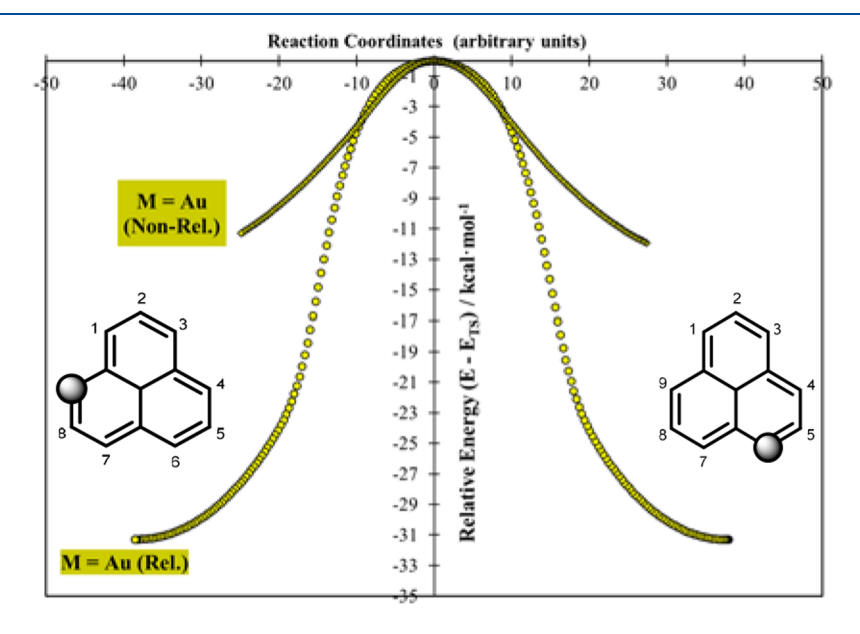


Figure 7. IRC paths for PAu for Pathway 3' with and without relativistic Au basis set and ECP.

Organometallics Article Article

and S2a), and (ii) toward C(1) two carbon atoms away in the other case (Figures 4a, and S2b). The former is in line with pathway 3' (Figure 4b), and the latter is in line with pathway 3a (Figure 4a). So both channels appear to be accessible to the η^1 PM systems for M = Cu, Ag, as well as Au, but, as we discuss shortly, orbital or shell effects—independent of relativistic effects or any structural change that occurs when we substitute for Au—seem to account for the anomaly.

Incidentally, an interesting observation from the graphic depicting low frequency vibrations of PAu in Figure S2 is that a noticeable out of plane distortion of the phenalenyl ring is associated with the transfer of the metal atom from C(9) to C(6) and from C(9) to C(1). The actual vibrational amplitudes will depend on temperature, but sample movies of the IRC paths for pathways 1, 2, 3a,b, and 3', which are included in the Supporting Information, indicate that the extent of the out of plane distortion accompanying shifts from one carbon center to another is somewhat more substantial for the shifts of the (η^1) M-C σ -bonds for pathways 3 and 3' relative to the distortions for pathways 1 and 2 from one high hapticity to another. This is well in line with the relatively low costs that we have computed for rearrangements of the group 1 metals on P.

Orbital Perspectives. Figure 8 shows sample HOMOs for the transition state geometries for pathways 3 and 3', using

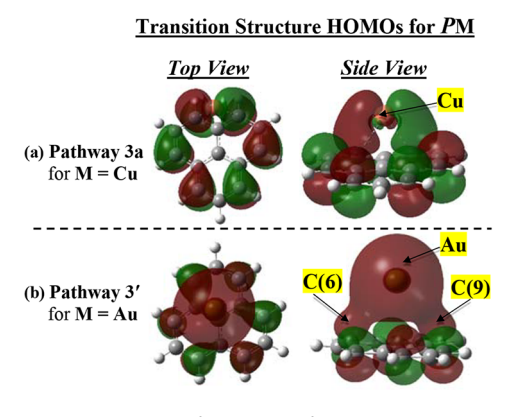


Figure 8. Representations of HOMOs of group 11 PM transition state structures.

*P*Cu for pathway 3a and *P*Au for pathway 3'. For pathway 3a, the highest occupied molecular orbitals (HOMOs) of the transition state structures (see *P*Cu in Figure 8) involve—on the metal center specifically—a *p*- or *d*-orbital that bridges out-of-phase π -type MO fragments on the ring on either side of the recess region (see top and side views for "Pathway 3a" in Figure 8). For the TS for pathway 3', however, (shown for M = Au in Figure 8), the jump between C(6) and C(9) is mediated only by an *s*-orbital on Au (Figure 8; bottom).

A simplified picture of key orbital interactions in the transition state HOMOs shown in Figure 8 is provided in Figure S3. We find that a quantitative assessment of the orbital contributions to the bonding in the two different types of transition states for pathways 3 and 3' affirm the observations in Figure 8 and the simplifications offered in Figure S3. Using the ADF software and the preoptimized transition structures, we carried out a bonding analysis in which we treated the M atom and P as neutral fragments. The results presented in Table 3 show that for M = Cu and Ag, P makes the dominant contribution to the bonding with far smaller contributions

Table 3. M Orbital Contributions to the Overall HOMO of the Transition Structures (TSs) for Pathways 3a and 3'a

	% M for TS (Pathway	% M for TS (Pathway 3')					
	<i>d</i> -orbital	p-orbital		s-orbital	<i>p</i> -orbital		
Cu	1.4% 3d _{xy} ; 1.1% 3d _{yz}	6.1% 4p _y	Cu	15.3% 4s	$1.5\%~4\mathrm{p}_z$		
Ag	2.0% 4d _{yz}	4.6% 4p _y	Ag	27.6% 5s	_		
Au	_	_	Au	61.2% 6s	_		
a Only the M contributions are shown. % phenalenyl = 100% $-$ % M.							

from the (n-1)d and np orbitals on M for pathway 3a, and the ns-orbital as well for pathway 3'.

For PAu, however, the Au valence s-orbital contribution dominates the bonding: P contributing only 38.8%, compared to over 70% at least in the cases for Cu and Ag (Table 3). Despite the huge involvement of Au in the MO, no p or d involvement is observed. Au is known to hop, for example, around the edge of Cp in the η^1 CpAu complex, 31,32 and that kind of "ring-whizzing" in cyclopentadienyl compounds is believed to also engage (n-1)d, and np orbitals. Moreover, as shown in Figure S6 and S7, computed relativistic activation free energies below 10 kcal·mol⁻¹ (7.8 and 9.1 kcal·mol⁻¹ at different levels of theory) are obtained for the shift of Au from one carbon center to its neighbor in Cp. So it is a bit surprising that pathway 3 (i.e., 3a + 3b) is avoided for PAu, even though for pathway 3' the PAu activation barrier is much higher than 10 kcal·mol⁻¹ (Figure 5). Yet the spacings of the secondary carbon centers are clearly quite different in P compared to Cp, as are the locations of the p orbitals in their frontier MOs, and the size and symmetry of the two rings. As a consequence, we find, two rather dramatic isomerization pathways are accessible for Au in PAu that involved primarily its valence s-orbital (Figures 4b and 6), allowing Au to go across or even below the phenalenyl ring rather than smoothly around it.

A look at an interaction diagram for the transition states for pathway 3' helps us to see why that path might be disfavored by Cu but favored by Au (Figure S4). The overlap of the Cu ns-orbital with the in-phase p-orbitals that are far from it on the other side of P is rather poor (consider, e.g., the Cu case in Figure S4 and general model in Figure S3), but, as M gets bigger, the overlap improves significantly, especially at M = Au (Figures 8 and S4). Additionally, the Au s-orbital is much lower in energy than the phenalenyl SOMO (Figure S4)—well in line with the high %s contribution seen in Table 3—leading to the greatest transition state HOMO stabilization of the three cases (see Figure S4), and evidently a definite preference for this pathway for the traversal of the ring compared to the alternative that we have identified for M = Cu and Ag.

■ SUMMARY AND OUTLOOK

Interest in the potential applications of the phenalenyl radical and its ions in materials engineering and related areas, including the design of spin-based memory devices and molecular magnets, remains substantial. But progress in exploring fundamental aspects of and linking these features to the electronic properties and structural preferences in compounds of that intriguing tricyclic hydrocarbon has been slow. The structure, bonding, and energetics of alkali metal complexes of the radical are examined for the first time for groups 1 and 11 metals and remarkably low barriers are identified for all of the group 1 systems, especially for those below Li. The latter is shown to adopt η^3 and η^6 hapticities on

the phenalenyl surface, and barriers to haptotropic rearrangements are quantified for all of the systems considered. For group 11 metals, the η^1 bonding preferences are clear; the relative magnitudes of barriers to translocation on the phenalenyl surface are even more substantial for Cu, Ag, and Au, compared to the Li case.

For Au, relativistic effects account for more than 50% of the barrier, but—even without relativistic effects—we find that orbital effects dictate that certain modes of motion available to copper and silver on *P* are effectively forbidden for gold.

The relatively large barriers obtained for Au compared to the other systems considered in this work mean that it will likely be, under experimental conditions, the least fluxional or most easily controlled kinetically of the group 11 *PM* systems. We have not found any report on attempts to synthesize the sets of *PM* systems discussed in this contribution, but the established syntheses of certain group 1 CpM compounds^{22–24} and CpAu^{31,32} may be a source for both strategies and inspiration for the experimental examinations of these compounds including the unusual Li and Au systems.

COMPUTATIONAL METHODS

The geometrical data, harmonic vibrational frequencies, and internal reaction coordinate (IRC) paths reported in this work have been obtained using the Becke three parameter hybrid exchange, and Perdew–Wang correlation functional (B3PW91)^{33,34} as implemented in the Gaussian 09 (G09) suite of programs³⁵ unless stated otherwise. The correlation-consistent triple- ζ (cc-pVTZ) basis sets³⁶ were employed for all elements, except for K, Rb, Cs, Ag and Au. For the heavy main group elements, the relativistic small core Stuttgart-Cologne Dirac–Fock (MDF) effective core potentials (ECPs) and the associated 9-valence-electron basis sets were employed.^{37,38} MDF ECPs were used as well³⁹ for Ag and Au along with the relevant triple- ζ 19-valence basis sets,^{39,40} and the nonrelativistic Hartree–Fock (MHF) ECPs and basis sets⁴¹ enabled us to assess by contrast the influence of relativistic effects on the bonding of Ag and Au.

The molecular representations and orbital pictures were generated using the Chemcraft, ⁴² Gaussview, ⁴³ and Chemdraw programs. The Synchronous Transit-guided Quasi-Newton method as implemented in the G09 software—both the QST2 and QST3 options—were employed to identify putative transition structures (TSs) linking established minima on the potential energy surface (PES) of PM complexes. Candidate transition structures generated in that way were reoptimized, confirmed to be first order saddle points, and used as starting points for internal reaction coordinate (IRC) path calculations in order to obtain a refined picture of the translation of M across the surface of P.

For the IRC calculations, we used high "maxpoints" values in each case such that the IRC path calculations terminated before any limit on the number of points was reached. IRC path calculations do not necessarily terminate at actual minimum energy geometries, so all IRC end points were fully optimized in separate calculations and confirmed by harmonic vibrational frequency analyses to be minima. Wiberg bond indices that we report have been obtained from natural bond orbital (NBO) analyses on the optimized geometries using the NBO 3.1 program as implemented in the G09 suite. The fragment analysis feature of the Amsterdam Density Functional (ADF) software 44-46 has been used to gain some insight into the bonding in previously optimized PM structures. Those calculations were done at the B3LYP level along with the triple- ζ quality (TZP) all electron basis sets with scalar relativistic effects included for all atoms. The B3PW91 model chemistry, which we used predominantly in this work, 47 was unavailable in the ADF suite, hence our choice of the B3LYP method for the latter analysis. The selected methods and triple- ζ basis sets have been employed because of their extensive use in the chemical literature and their overall reliability as model chemistries for computing structural and energetic data for inorganic

and organometallic systems. We have also assessed the qualitative reliability of our results, however, by recomputing our structural and IRC data using the $\omega \rm B97XD$ method. 48

ASSOCIATED CONTENT

S Supporting Information

The Supporting Information is available free of charge at https://pubs.acs.org/doi/10.1021/acs.organomet.9b00564.

Coordinates and pictures of optimized minima and transition states, Bond order and bond distance data, Graphical representations of orbital interactions, vibrational motions, and comparisons of reaction coordinates with and without relativistic effects, and Interaction diagrams (PDF)

Videos for haptotropic rearrangements and isomerizations (ZIP)

Cartesian coordinates in special format (XYZ)

AUTHOR INFORMATION

Corresponding Author

*Tel.: 804-484-1628. Fax: 804-287-1897. E-mail: kdonald@richmond.edu.

ORCID

Kelling J. Donald: 0000-0001-9032-4225

Notes

The authors declare no competing financial interest.

ACKNOWLEDGMENTS

Our work was supported by the National Science Foundation: NSF-CAREER Award (CHE-1056430) and NSF-MRI Grants (CHE-0958696 (University of Richmond (UR)) and CHE-1229354 (the MERCURY consortium)). S.P., and M.H. thank the NSF and Research Corporation, respectively, for summer research support. N.W. acknowledges the Howard Hughes Medical Institute for support through the URISE and SMART programs at UR. K.J.D. acknowledges the support of the Henry Dreyfus Teacher-Scholar Awards Program.

REFERENCES

- (1) Reid, D. H. Stable π -Electron Systems and New Aromatic Structures. *Tetrahedron* **1958**, *3*, 339–352.
- (2) Reid, D. H. The Chemistry of the Phenalenes. Q. Rev., Chem. Soc. **1965**, 19, 274–302.
- (3) Ahmed, J.; Sreejyothi, P.; Vijaykumar, G.; Jose, A.; Raj, M.; Mandal, S. K. A New Face of Phenalenyl-Based Radicals in the Transition Metal-Free C-H Arylation of Heteroarenes at Room Temperature: Trapping the Radical Initiator via C-C σ -Bond Formation. *Chem. Sci.* **2017**, *8*, 7798–7806.
- (4) Mukherjee, A.; Sau, S. C.; Mandal, S. K. Exploring Closed-Shell Cationic Phenalenyl: From Catalysis to Spin Electronics. *Acc. Chem. Res.* **2017**, *S0*, 1679–1691.
- (5) Toader, A. M.; Buta, C. M.; Frecus, B.; Mischie, A.; Cimpoesu, F. Valence Bond Account of Triangular Polyaromatic Hydrocarbons with Spin: Combining Ab Initio and Phenomenological Approaches. *J. Phys. Chem. C* **2019**, *123*, 6869–6880.
- (6) The case where n=1, for the n-triangulenes $C_{(n^2+4n+1)}H_{(3n+3)}$, is benzene, which is not a radical. The number of radical electrons for a given system is n-1, so the first physically meaningful case is n=2, i.e., the phenalenyl radical. The case where n=0 is a radical, \bullet CH₃, but not a ring.
- (7) Mukherjee, A.; Sen, T. K.; Ghorai, P. K.; Mandal, S. K. The Non-Innocent Phenalenyl Unit: An Electronic Nest to Modulate the Catalytic Activity in Hydroamination Reaction. *Sci. Rep.* **2013**, 3, 2821.

(8) Raman, K. V.; Kamerbeek, A. M.; Mukherjee, A.; Atodiresei, N.; Sen, T. K.; Lazić, P.; Caciuc, V.; Michel, R.; Stalke, D.; Mandal, S. K.; Blügel, S.; Münzenberg, M.; Moodera, J. S. Interface-Engineered Templates for Molecular Spin Memory Devices. *Nature* **2013**, 493, 509–513.

- (9) Pal, S. K.; Bag, P.; Itkis, M. E.; Tham, F. S.; Haddon, R. C. Enhanced Electrical Conductivity in a Substitutionally Doped Spiro-Bis(Phenalenyl)Boron Radical Molecular Solid. *J. Am. Chem. Soc.* **2014**, *136*, 14738–14741.
- (10) Cui, Z.; Lischka, H.; Beneberu, H. Z.; Kertesz, M. Rotational Barrier in Phenalenyl Neutral Radical Dimer: Separating Pancake and van Der Waals Interactions. *I. Am. Chem. Soc.* **2014**, *136*, 5539–5542.
- (11) Uchida, K.; Mou, Z.; Kertesz, M.; Kubo, T. Fluxional σ -Bonds of the 2,5,8-Trimethylphenalenyl Dimer: Direct Observation of the Sixfold σ -Bond Shift via a π -Dimer. *J. Am. Chem. Soc.* **2016**, *138*, 4665–4672.
- (12) Kubo, T. Synthesis, Physical Properties, and Reactivity of Stable, π -Conjugated, Carbon-Centered Radicals. *Molecules* **2019**, 24, 665.
- (13) Koutentis, P. A.; Chen, Y.; Cao, Y.; Best, T. P.; Itkis, M. E.; Beer, L.; Oakley, R. T.; Cordes, A. W.; Brock, C. P.; Haddon, R. C. Perchlorophenalenyl Radical. *J. Am. Chem. Soc.* **2001**, *123*, 3864–3871.
- (14) Goto, K.; Kubo, T.; Yamamoto, K.; Nakasuji, K.; Sato, K.; Shiomi, D.; Takui, T.; Kubota, M.; Kobayashi, T.; Yakusi, K.; et al. A Stable Neutral Hydrocarbon Radical: Synthesis, Crystal Structure, and Physical Properties of 2,5,8-Tri-Tert-Butyl-Phenalenyl. *J. Am. Chem. Soc.* 1999, 121, 1619.
- (15) Mou, Z.; Uchida, K.; Kubo, T.; Kertesz, M. Evidence of σ and π -Dimerization in a Series of Phenalenyls. *J. Am. Chem. Soc.* **2014**, 136, 18009–18022.
- (16) Uchida, K.; Hirao, Y.; Kurata, H.; Kubo, T.; Hatano, S.; Inoue, K. Dual Association Modes of the 2,5,8-Tris(pentafluorophenyl)-phenalenyl Radical. *Chem. Asian J.* **2014**, *9*, 1823–1829.
- (17) Craciun, S.; Donald, K. J. Radical Bonding: Structure and Stability of Bis(Phenalenyl) Complexes of Divalent Metals from across the Periodic Table. *Inorg. Chem.* **2009**, *48*, 5810–5819.
- (18) The significant polarity of the PM molecule is in line with the well-established ionic character of group 1 CpM compounds. The structures of a number of group 1 CpM compounds in the solid state is discussed in chapters 5 and 15 (specifically the introduction to 15.4.3, and section 15.4.3.1) of reference 19.
- (19) Elschenbroich, C. Organometallics, 3rd ed.; Wiley-VCH: Weinheim, Germany, 2006.
- (20) Nixon, D. E.; Parry, G. S. Formation and Structure of the Potassium Graphites. J. Phys. D: Appl. Phys. 1968, 1, 291–299.
- (21) Perez-Peralta, N.; Contreras, M.; Tiznado, W.; Stewart, J.; Donald, K. J.; Merino, G. Stabilizing Carbon-Lithium Stars. *Phys. Chem. Chem. Phys.* **2011**, *13*, 12975–12980.
- (22) Thiele, J. Ueber Abkömmlinge des Cyclopentadiëns. Cyclopentadiënkalium (On the Derivatives of Cyclopentadienyl. Cyclopentadienylpotassium). *Ber. Dtsch. Chem. Ges.* **1901**, *34*, 68–71.
- (23) Dinnebier, R. E.; Behrens, U.; Olbrich, F. Solid State Structures of Cyclopentadienyllithium, -Sodium, and -Potassium. Determination by High-Resolution Powder Diffraction. *Organometallics* **1997**, *16* (17), 3855–3858.
- (24) Panda, T. K.; Gamer, M. T.; Roesky, P. W. An Improved Synthesis of Sodium and Potassium Cyclopentadienide. *Organometallics* **2003**, *22*, 877–878.
- (25) Meyer, F.; Khan, F. A.; Armentrout, P. B. Thermochemistry of Transition Metal Benzene Complexes: Binding Energies of M- $(C_6H_6)^{x+}$ (x = 1, 2) for M = Ti to Cu. *J. Am. Chem. Soc.* **1995**, 117, 9740–9748.
- (26) Delbaere, L. T. J.; McBride, D. W.; Ferguson, R. B. The Crystal Structure of π -Cyclopentadienyl(triethylphosphine)copper(I), π -C₅H₅CuP(C₂H₅)₃. Acta Crystallogr., Sect. B: Struct. Crystallogr. Cryst. Chem. 1970, B26, 515–521.

(27) Parvin, N.; Pal, S.; Echeverría, J.; Alvarez, S.; Khan, S. Taming a Monomeric $[Cu(\eta^6\text{-C6H6})]^+$ Complex with Silylene. *Chem. Sci.* **2018**, *9*, 4333–4337.

- (28) Tian, Y. H.; Kertesz, M. Bimolecular Hydrogen Transfer in Phenalene by a Stepwise Ene-like Reaction Mechanism. *Chem. Commun.* **2010**, *46*, 4282–4284.
- (29) Pyykkö, P. Relativistic Effects in Structural Chemistry. Chem. Rev. 1988, 88, 563-594.
- (30) Schwarz, W. H. E. Fundamentals of Relativistic Effects in Chemistry. In *Theoretical Models of Chemical Bonding, Part 2: The Concept of the Chemical Bond*; Maksic, Z. B., Ed.; Springer: Berlin, 1990.
- (31) Hüttel, R.; Raffay, U.; Reinheimer, H. Cyclopentadienylgold(I) and Cyclopentadienyl(triphenylphosphine)gold(I)Angew. *Angew. Chem., Int. Ed. Engl.* **1967**, *6*, 862; *Angew. Chem.* **1967**, *79*, 859–860.
- (32) Smyslova, E. I.; Perevalova, E. G.; Dyadchenko, V. P.; Grandberg, K. I.; Slovokhotov, Yu. L.; Struchkov, Yu. T. Syntheses of Organogold(1+) Compounds by Direct Auration. *J. Organomet. Chem.* **1981**, 215 (2), 269–279.
- (33) Becke, A. D. Density-functional thermochemistry. III. The role of exact exchange. *J. Chem. Phys.* **1993**, *98*, 5648–5652.
- (34) Perdew, J. P.; Burke, K.; Wang, Y. Generalized Gradient Approximation for the Exchange-Correlation Hole of a Many-Electron System. *Phys. Rev. B: Condens. Matter Mater. Phys.* **1996**, 54, 16533–16539 and references therein.
- (35) Frisch, M. J.; Trucks, G. W.; Schlegel, H. B.; Scuseria, G. E.; Robb, M. A.; Cheeseman, J. R.; Scalmani, G.; Barone, V.; Petersson, G. A.; Nakatsuji, H.; et al. *Gaussian 09*, Revision D.01; Gaussian, Inc.: Wallingford, CT, 2016.
- (36) Dunning, T. H. Gaussian Basis Sets for Use in Correlated Molecular Calculations. I. The Atoms Boron through Neon and Hydrogen. *J. Chem. Phys.* **1989**, *90*, 1007–1023.
- (37) Stuttgart—Cologne basis set is available online at the following website: http://www.tc.uni-koeln.de/PP/clickpse.en.html (last accessed June 15, 2019).
- (38) Lim, I. S.; Schwerdtfeger, P.; Metz, B.; Stoll, H. All-Electron and Relativistic Pseudopotential Studies for The Group 1 Element Polarizabilities from K to Element 119. *J. Chem. Phys.* **2005**, 122, 104103
- (39) Figgen, D.; Rauhut, G.; Dolg, M.; Stoll, H. Energy-Consistent Pseudopotentials for Group 11 and 12 Atoms: Adjustment to Multi-Configuration Dirac-Hartree-Fock Data. *Chem. Phys.* **2005**, *311*, 227–244.
- (40) Peterson, K. A.; Puzzarini, C. Systematically Convergent Basis Sets for Transition Metals. II. Pseudopotential-Based Correlation Consistent Basis Sets for The Group 11 (Cu, Ag, Au) and 12 (Zn, Cd, Hg) Elements. *Theor. Chem. Acc.* 2005, 114, 283–296.
- (41) Schwerdtfeger, P.; Dolg, M.; Schwarz, W. H. E.; Bowmaker, G. A.; Boyd, P. D. W. Relativistic Effects in Gold Chemistry. I. Diatomic Gold Compounds. *J. Chem. Phys.* **1989**, *91*, 1762–1774.
- (42) Andrienko, A. G.; Senchenya, I. N.; Romanov, A. Chemcraft (A Graphical User Interface for Computational Chemistry Programs); http://www.chemcraftprog.com.
- (43) Dennington, R.; Keith, T. A.; Millam, J. M. *GaussView*, Version 6; Semichem Inc.: Shawnee Mission, KS, 2016.
- (44) Fonseca Guerra, C.; Snijders, J. G.; te Velde, G.; Baerends, E. J. Towards an Order-N DFT Method. *Theor. Chem. Acc.* **1998**, *99*, 391–403.
- (45) te Velde, G.; Bickelhaupt, F. M.; Baerends, E. J.; Fonseca Guerra, C.; van Gisbergen, S. J. A.; Snijders, J. G.; Ziegler, T. Chemistry with ADF. J. Comput. Chem. 2001, 22, 931–967.
- (46) ADF 2013, SCM, Theoretical Chemistry; Vrije Universiteit: Amsterdam, The Netherlands, http://www.scm.com.
- (47) The B3PW91 method was used because we have found it to give good agreement with experiments on structural parameters for inorganic and organometallic systems.
- (48) Chai, J.-D.; Head-Gordon, M. Long-range corrected hybrid density functionals with damped atom-atom dispersion corrections. *Phys. Chem. Phys.* **2008**, *10*, 6615–6620.